The Astronomical Journal, 124:1706–1715, 2002 September

ANGULAR SIZE MEASUREMENTS OF MIRA VARIABLE STARS AT 2.2 MICRONS. II.

G. T. van Belle, R. R. Thompson, and M. J. Creech-Eakman[1]
Jet Propulsion Laboratory, MS 171-113, California Institute of Technology, 4800 Oak Grove Drive, Pasadena, CA 91109;
gerard@huey.jpl.nasa.gov
Received 2002 March 20; accepted 2002 June 11

ABSTRACT

We present angular size measurements of 22 oxygen-rich Mira variable stars. These data are part of a long-term observational program using the Infrared Optical Telescope Array to characterize the observable behavior of these stars. Complementing the infrared angular size measurements, values for variable star phase, spectral type, bolometric flux, and distance were established for stars in the sample; flux and distance led to values for effective temperature ($T_{\rm eff}$) and linear radius, respectively. Additionally, values for the $K-[12]$ color excess were established for these stars, which is indicative of dusty mass loss. Stars with higher color excess are shown to be systematically 120 $R_{\odot}$ larger than their low color excess counterparts, regardless of period. This analysis appears to present a solution to a long-standing question presented by the evidence that some Mira angular diameters are indicative of first-overtone pulsation, while other diameters are more consistent with fundamental pulsation. A simple examination of the resultant sizes of these stars in the context of pulsation mode is consistent with at least some of these objects pulsating in the fundamental mode.

Key words: infrared radiation — Miras — stars: fundamental parameters — stars: late-type — techniques: interferometric

On-line material: color figures

1. INTRODUCTION

The recent development of interferometric methods at optical and infrared wavelengths has provided the astronomical community with more than an order of magnitude increase in spatial resolution over direct imaging techniques. Using the Infrared Optical Telescope Array (IOTA; see Carleton et al. 1994 and Dyck et al. 1995) and the Palomar Testbed Interferometer (PTI; see Colavita et al. 1999), we have been conducting a program of high-resolution, *K*-band observations of Mira variable stars. Previous IOTA results have been presented for both oxygen-rich Miras (van Belle et al. 1996) and carbon and S-type Miras and non-Mira S-type stars (van Belle et al. 1997).

Mira variables figure prominently in our observing strategy, since these stars are large and bright at infrared wavelengths. Using crude estimates of surface temperatures and the observed total fluxes, it is estimated that more than 100 such stars have blackbody angular diameters in excess of 2 mas, easily resolvable targets for the current generation of Michelson interferometers. The 22 stars reported herein represent a significant collection of angular sizes to be added to the literature, roughly doubling the number of sizes available. This large sample allows for a more detailed analysis of the behavior of these stars.

Recent investigations of Mira variables have attempted to resolve important questions regarding the pulsation mode, mass loss, and evolution of these stars. The pulsation mode remains a currently unresolved issue; the promise of high-resolution interferometric methods to firmly resolve this question is hampered by conflicts between distance determination methods. Initial studies of these stars in the visible (Haniff, Scholz, & Tuthill 1995; Lattanzi et al. 1997; Burns et al. 1998; Young et al. 2000) and infrared (van Belle et al. 1996, 1997; Perrin et al. 1999; Hofmann et al. 2002; Thompson, Creech-Eakman, & van Belle 2002b) have yet to provide conclusive evidence in favor of fundamental versus first-overtone pulsation mode, although a deeper understanding of these complex and dynamic stellar atmospheres is beginning to emerge as a direct result of these investigations.

Studies attempting to derive distances to Miras, independent of assumptions about pulsation mode, fail to reach agreement on the subject. Whitelock & Feast (2000), using parallax data from *Hipparcos* to derive a *K*-band period-luminosity relation, which, in conjunction with Mira angular size data and published model atmospheres, they find to indicate a common first-overtone mode for most Miras. The resultant LMC distance modulus Whitelock & Feast derive is 18.64 ± 0.14, which is consistent with similar determinations using Cepheids (Groenewegen 2000) but in conflict with recent LMC distances as indicated by eclipsing binaries (Nelson et al. 2000; Ribas et al. 2000; Groenewegen & Salaris 2001) that favor smaller distance modulus values of 18.46 ± 0.06 or less. In contrast to that investigation, Alvarez & Mennessier (1997), using TiO and VO band strengths, arrive at radii and temperatures that favor fundamental pulsations. This finding is in agreement with the group of Wood et al. (1999); Wood (2000), who examines Mira period ratios found in MACHO data to argue strongly in favor of fundamental mode. Depending upon initial assumptions, models supporting both fundamental-mode pulsation (Willson & Hill 1979; Hill & Willson 1979; Wood 1990) and first-overtone pulsation (Wood 1974; Tuchman, Sack, & Barkat 1979; Perl & Tuchman 1990) have been constructed, in certain cases, the pulsation mode itself is a free parameter (Hofmann, Scholz, & Wood 1998).

It is by means of direct observation of the angular sizes of Mira variables that we may be able to provide unique insight into these questions. Additional information in the form of bolometric flux estimates will yield further

[1] Caltech/JPL Postdoctoral Scholar.

information, such as effective temperature, which remains a poorly established quantity for this class of stars. In addition, our angular size measurements and derived quantities have implications regarding the nature of mass loss and evolution among Mira variables.

Carbon-rich, oxygen-rich, and S-type Miras were all observed at IOTA and PTI as a part of our ongoing high-resolution program; in this paper, we present only the observations of the oxygen-rich variety observed at IOTA. Observations at IOTA using the related FLUOR experiment are not considered in this article as part of the data set (Perrin et al. 1999), although they are in agreement with our conclusions, particularly that of fundamental-mode pulsation for Miras (Hofmann et al. 2002). Operations at IOTA that produced these results are discussed in § 2, detailing source selection and observation. In § 3, the procedures used in establishing the stellar parameters for the stars observed are discussed; the parameters include phase, spectral type, bolometric flux, angular size, effective temperature, and linear radius. These parameters are, in turn, examined for significant interrelationships in the discussion of § 4.

2. OBSERVATIONS

The data reported in this paper were obtained in the K band ($\lambda = 2.2$ μm, $\Delta\lambda = 0.4$ μm) at IOTA, using the 21 and 38 m baselines. Use of IOTA at 2.2 μm to observe Mira variables offers three advantages: First, effects of interstellar reddening are minimized, relative to the visible ($A_K = 0.11A_V$; Mathis 1990); second, the effects of circumstellar emission are minimized shortward of 10 μm (Rowan-Robinson & Harris 1983); and third, the K-band apparent uniform-disk diameter of Mira variables has in the past been expected to be close to the $\tau = 1$ Rosseland mean photospheric diameter (see the discussions in §§ 3.3 and 4). The interferometer, detectors, and data reduction procedures have been described more fully by Carleton et al. (1994) and Dyck et al. (1995). As was previously reported in these papers, starlight collected by the two 0.45 m telescopes is combined on a beam splitter and detected by two single-element InSb detectors, resulting in two complementary interference signals. The optical path delay is mechanically driven through the white-light fringe position to produce an interferogram with fringes at a frequency of 100 Hz. Subsequent data processing locates the fringes in the raw data and filters out the low- and high-frequency noise with a square filter 50 Hz in width. Recent software and hardware upgrades to the computers driving the interferometer and collecting the data have resulted in a improved data collection rate to 1500–2000 fringe packets per night. On the best nights, we can observe 20 science sources and an equal number of calibrators.

Observations of target objects are alternated with observations of unresolved calibration sources to characterize slight changes in interferometer response (no more than a few percent) due to both seeing and instrumental variations. Raw visibilities are determined from the amplitude of the interferogram at the white-light fringe position, normalized by the incoherent flux from the star. An estimate of the noise is obtained from a similar measurement made in the data outside the region of coherence; the noise estimate is used in obtaining a weighted average of the visibility data, which is typically taken in sets of 50 interferograms. The raw visibilities of the target objects are then calibrated by dividing them by the measured visibilities of the calibration sources, using the calibration sources as samples of the interferometer's point response. Calibration sources were selected from V-band data available in the Bright Star Catalog (Hoffleit & Jaschek 1982) and K-band data in the Catalog of Infrared Observations (Gezari et al. 1993), based upon angular sizes calculated from estimates of bolometric flux and effective temperature; calibration source visibility was selected to be at least 90% and ideally greater than 95%, limiting the effect of errors in calibrator visibility to a level substantially below measurement error.

Mira variables observed for this paper were selected based upon a number of criteria. Stars needed to be bright enough in V and K to be detected by both the star trackers and the InSb detectors; the current limits of the IOTA interferometer dictate $V < 8.0$ mag and $K < 5$ mag (although for observations at all air masses and seeing conditions, we require $K < 2.5$ mag). The Mira variables needed to be at a declination accessible to the mechanical delay available for a given evening. This is because the difference in delay between the two apertures, which can range from -30 to $+20$ m, depends upon source declination and hour angle. Since only 4.6 m of this range is accessible at any time, observing is constrained to a specific declination bin about 10° wide on any given night. The stars also needed to be of sufficient estimated angular size to be resolved by IOTA. Mira phase was not a factor in target selection; hence, our targets represent Miras at a variety of phases, from visible light maximum to minimum.

Twenty-two oxygen-rich Mira variables were observed at IOTA during four observing runs in March, May–June, and October of 1996 and July of 1997. The visibility data for the two detector channels have been averaged and are listed in Table 1, along with the date of the observation, the interferometer projected baseline, the stellar phase, and the derived uniform disk angular size; the latter two points are discussed further in § 3. In our experience with the IOTA interferometer, Dyck et al. (1996) has demonstrated that the night-to-night rms fluctuations in visibility data generally exceed the weighted statistical error from each set of interferograms; we have characterized these fluctuations and use the empirical formula $\sigma_V = \pm 0.051/\sqrt{N}$ (number of nights) to assign the "external" error. The interested reader should see Dyck et al. (1996) for a more complete discussion. Finally, visibility data were fitted to uniform disk models to obtain an initial angular size $\theta_{\rm UD}$. These uniform disk diameters and their estimated errors, derived from the uncertainty in the visibilities, are also listed in Table 1.

We note that typically a single point was used in calculating the uniform disk diameter $\theta_{\rm UD}$. For the stars in our sample, the visibility data were all at spatial frequencies, x, shortward of the first zero of the uniform disk model, $|2J_1(x)/x|$, where $x = \pi\theta_{\rm UD}B/\lambda$. Haniff et al. (1995) noted that the uniform disk model was not a particularly good model for visible light data for Mira variables; rather, the data were a better fit to a simple Gaussian. Although we do not currently have multiple spatial frequency data for any Mira variables, our naive expectation, as followed in van Belle et al. (1996, 1997), was that the departures from a uniform disk model will not be as great at 2.2 μm as they are at visible wavelengths. This expectation appears to be borne out by comparisons of the data for R Aqr by van Belle et al.

TABLE 1
OBSERVED DATA

Star	Period P	$\phi = 0$ JD	Obs. Date	Obs. JD	Phase ϕ	B_P (m)	V[a]	θ_{UD} (mas)
RR Aql	399.8	50,046	1996 Jun 4	50,239	0.48	31.13	0.465	10.73 ± 0.66
RT Aql.....	328.6	49,875	1996 Jun 3	50,238	0.10	37.00	0.705	7.24 ± 0.42
			1996 Jun 7	50,242	0.12	35.45	0.582	
V Cam.....	524.5	50,190	1996 Oct 9	50,366	0.34	26.57	0.759	8.36 ± 0.40
			1996 Oct 9	50,366	0.34	27.41	0.740	
			1996 Oct 9	50,366	0.34	28.04	0.663	
			1996 Oct 9	50,366	0.34	28.64	0.692	
V Cas	226.6	50,289	1996 Oct 6	50,363	0.33	34.69	0.740	6.30 ± 0.66
Y Cas	410.7	50,303	1996 Oct 7	50,364	0.15	35.95	0.643	7.28 ± 0.59
S CrB	359.5	49,725	1996 Mar 7	50,150	0.18	21.21	0.754	11.35 ± 0.26
			1996 Mar 7	50,150	0.18	21.21	0.662	
			1996 Mar 7	50,150	0.18	21.21	0.726	
			1996 Mar 8	50,151	0.19	21.21	0.663	
			1996 Mar 8	50,151	0.19	21.21	0.641	
			1996 Mar 8	50,151	0.19	21.21	0.639	
			1996 Mar 8	50,151	0.19	21.21	0.619	
			1996 Mar 8	50,151	0.19	21.21	0.611	
			1996 Mar 8	50,151	0.19	21.21	0.555	
			1996 Mar 8	50,151	0.19	21.20	0.598	
			1996 Mar 12	50,155	0.20	38.22	0.357	
			1996 Mar 12	50,155	0.20	38.21	0.368	
R CVn.....	329.2	50,150	1996 Mar 13	50,156	0.02	37.00	0.681	6.63 ± 0.59
			1996 May 29	50,233	0.25	37.60	0.583	7.66 ± 0.28
			1996 May 30	50,234	0.26	37.57	0.590	
			1996 May 30	50,234	0.26	37.66	0.599	
			1996 Jun 7	50,242	0.28	35.52	0.581	
BG Cyg	287.7	49,524	1996 Jun 7	50,242	0.50	35.45	0.877	4.14 ± 0.83
DG Cyg	463.9	49,891	1996 May 29	50,233	0.74	36.80	0.784	5.36 ± 0.66
R Dra.....	246.0	50,431	1997 Jul 5	50,635	0.83	20.90	0.658	12.04 ± 1.36
			1997 Jul 5	50,635	0.83	20.57	0.692	
RU Her.....	485.6	49,800	1996 Jun 2	50,237	0.90	37.58	0.507	8.71 ± 0.39
			1996 Jun 3	50,238	0.90	37.57	0.457	
U Her.....	406.4	49,880	1996 Jun 2	50,237	0.88	37.31	0.263	11.18 ± 0.60
R LMi.....	372.8	49,600	1996 Mar 7	50,150	0.48	21.19	0.534	14.40 ± 0.66
			1996 Mar 7	50,150	0.48	21.19	0.668	
			1996 Mar 7	50,150	0.48	21.07	0.529	
			1996 Mar 7	50,150	0.48	21.05	0.552	
RT Oph.....	427.4	49,925	1996 Jun 7	50,242	0.74	35.16	0.717	6.52 ± 0.64
UU Peg	458.5	49,690	1996 Jun 3	50,238	0.20	36.96	0.417	9.56 ± 0.56
Z Peg.....	331.4	50,711	1996 Oct 4	50,361	0.94	37.64	0.838	4.50 ± 0.71
RR Per.....	390.1	50,039	1996 Oct 7	50,364	0.83	35.99	0.679	6.83 ± 0.61
U Per	317.5	50,165	1996 Oct 6	50,363	0.62	33.93	0.811	5.41 ± 0.75
BG Ser	394.8	48,450	1996 Jun 4	50,239	0.53	30.51	0.769	6.71 ± 0.78
S Ser.....	375.9	49,875	1996 Mar 11	50,154	0.74	36.98	0.733	5.51 ± 0.42
			1996 Mar 11	50,154	0.74	36.89	0.796	
			1996 Mar 11	50,154	0.74	36.89	0.796	
			1996 Jun 8	50,243	0.98	32.26	0.832	5.35 ± 0.82
S UMi	328.2	49,850	1996 Jun 6	50,241	0.19	26.67	0.752	7.98 ± 0.87
RS Vir.....	354.1	49,325	1996 Jun 10	50,245	0.60	32.38	0.683	7.54 ± 0.67
R Cas[b].....	430.8	50,940	1995 Oct 4	49,995	0.81	35.27	0.125	$22.03^{+2.13}_{-4.13}$
			1995 Oct 5	49,996	0.81	36.30	0.1273	

[a] Standard nightly error is $\Delta V = 0.0509$.
[b] R Cas data is reanalysis of visibility data from van Belle et al. 1996.

(1996) with the observations of Tuthill et al. (2000); although, as we shall see in § 4, this may not be entirely accurate. Thus, initially we will assume that to first order, a uniform disk model will also fit the Mira data; a slight correction to the derived angular sizes to account for this assumption will be discussed in § 3.3. In this case, a single spatial frequency point will uniquely and precisely determine the angular diameters for visibilities in the approximate range $0.25 \geq V \geq 0.75$. As we shall see in § 4, there is evidence that this approach does not properly account for the deviation of a uniform disk size from the Rosseland mean diameter. Properly examining this point may only be addressed by detailed multiple spatial frequency observations of the visibility curves.

3. STELLAR PARAMETERS

3.1. *Phase*

The phases of the Mira variables observed were established by means of two sources, following the procedure outlined in van Belle et al. (1996, 1997). Periods were initially obtained from the General Catalog of Variable Stars (GCVS; Kholopov et al. 1985). However, since the zero-phase date in the GCVS at the epoch of the observations was no less than 11 cycles old for our sample stars, visual brightness data available from the Association Française des Observateurs d'Etoiles Variables (AFOEV) was used in estimating a recent zero-phase date (E. Schweitzer 1998, private communication).

As an additional cross-check, Fourier analysis (as discussed in Scargle 1982 and Horne & Baliunas 1986) of the AFOEV data also provided period information, but used light-curve data that was more recent than that found in the GCVS. The periods from the GCVS and the AFOEV analysis agreed at the 1% level, corresponding to an average difference in period of 1 ± 4 days. With the agreement in periods, the zero-phase estimate was the larger uncertainty in phase determination, although this uncertainty was still small, averaging 6 days. Periods, determined from Fourier analysis of the AFOEV data, and phases for each of the Mira variables are presented in Table 1.

3.2. *Spectral Type and Bolometric Flux*

Bolometric fluxes ($F_{\rm bol}$) of the Mira variable stars were estimated from a relationship between $F_{\rm bol}$ and 2.2 μm flux (F_K), as established by Dyck, Lockwood, & Capps (1974). In order to obtain bolometric fluxes, K magnitudes were first estimated from the incoherent (off-fringe) flux levels present in the IOTA data. We obtained our standard-star photometric calibrations using the K-band measurements found in the Two-Micron Sky Survey (Neugebauer & Leighton 1969) for our nonvariable point-response calibration sources. Cross calibrator comparison of the published versus measured values for m_K indicates the IOTA photometry is consistent with the previous measures, with uncertainty being dominated by measurement scatter. No airmass corrections were applied since the calibrators were observed at nearly identical air masses as the Mira variables. In all cases, the bolometric fluxes were obtained from the absolute K fluxes through the observed relation

$$\log(F_K/F_{\rm bol}) = 0.017(V - K) - 0.74\ , \qquad (1)$$

which is the mean relationship derived from Dyck et al. (1974) for spectral types M5–M10. A 15% error bar was assigned to the resultant $F_{\rm bol}$ values, which is consistent with more detailed $F_{\rm bol}$ estimations done by Whitelock & Feast (2000). We note that the log $(F_K/F_{\rm bol})$–spectral type relationship also has a firm theoretical basis and may be seen in the "infrared flux method" calculations carried out by Blackwell & Lynas-Gray (1994). No reddening corrections were applied to obtain the bolometric fluxes. These were deemed unnecessary, since the typical magnitude of the corrections will be $\Delta m_K < 0.10$ mag (calculated from the empirical reddening determination of Mathis 1990 and from the A_V values given for local Miras in Whitelock, Marang, & Feast 2000), which is less than the rms K-band error, $\Delta m_K = 0.15$ mag.

In contrast to our previous paper on this subject (van Belle et al. 1996), spectral types were *not* inferred from the mean observation data of Lockwood & Wing (1971) or Lockwood (1972). We note instead that over the range of spectral types in question (M5–M9.8), the log $(F_K/F_{\rm bol})$ versus $V-K$ relationship is nearly flat, making the determination of $F_{\rm bol}$ robust despite possible errors in $V-K$ color. An uncertainty of one full magnitude in $V-K$ results in only a 4% difference in the determined $F_{\rm bol}$; we shall see in § 3.4 that this results in a negligible difference in the determined effective temperature. The errors in the K magnitudes are the standard deviations of the individual measurements on a given night. From the observed scatter in the $F_K/F_{\rm bol}$ relationship, we estimate an rms error of $\pm 13\%$ in $F_{\rm bol}$ from the use of the K magnitude; we estimate a further uncertainty of $\pm 5\%$ in the absolute calibration (Blackwell & Lynas-Gray 1994). The estimated error for $F_{\rm bol}$ in Table 2 is the quadrature sum of these contributions of 15%.

3.3. *True Angular Diameter*

In order to estimate effective temperatures, the uniform disk diameters in Table 1 needed to be converted to stellar diameters corresponding to the nonuniform extended atmospheres of the Mira variables. We used the model Mira atmospheres discussed in Hofmann et al. (1998, hereafter HSW98). We note that the HSW98 models did not account for the time for both shock-compressed material and material expanding between shocks to return to radiative equilibrium. These regions, with $T > T_{\rm RadEq}$ and $T < T_{\rm RadEq}$, respectively, can alter the brightness distribution profile and consequently alter the "true" angular sizes derived from the uniform disk (UD) diameters. Rather, HSW98 follows Bessel, Scholz, & Wood (1996) in the semiempirical adoption of an equilibrium temperature just behind the shock front. Dynamical atmosphere calculations have the potential to resolve these concerns (Bowen 1988; Bowen & Willson 1991); however, center-to-limb brightness profiles are not yet available for such calculations. The missing physics in the models have the potential to make for poor agreement between angular sizes derived at different wavelength bands.

Noting these concerns, here we shall use the HSW98 models as a sufficient expectation of the intensity distribution across the disk of a Mira variable to proceed with our analysis. Fortunately, as illustrated in HSW98, the K band is a particularly forgiving bandpass in which to work, and the differences between UD diameters and the Rosseland mean radiating surface is potentially small. Examining all of the HSW98 models, four of the six models (series Z, D, E, and O) were seen as most representative of the parameters that matched the Miras observed; specifically, examining the bolometric flux variations of the local Miras as seen in Whitelock & Feast (2000), the average $\Delta m_{\rm bol} = 0.73 \pm 0.25$, which compares well with the bolometric flux variations seen in those four models in HSW98. For those models, the rms difference between a uniform disk fit and the Rosseland mean diameter is 1.00 ± 0.04, which we shall use as a scaling factor from which Rosseland angular sizes can be derived from K-band UD diameters. Within the context of a unit scaling factor, the main quantitative impact upon the Rosseland mean diameter from the UD diameter is the slight increase in error because of the uncertainty in scaling factor. A scaling factor equal to unity is consistent with expectation that near-infrared uniform disk diameters should be reason-

TABLE 2
DERIVED PARAMETERS: BOLOMETRIC FLUX, ROSSELAND ANGULAR DIAMETER, EFFECTIVE TEMPERATURE, DISTANCE, AND LINEAR RADIUS

Star	Date	V	K	$V-K$	$F_{\rm bol}$ (10^{-8} ergs cm^{-2} s^{-1})	θ_R (mas)	$T_{\rm eff}$ (K)
RR Aql	1996 Jun 4	12.8	0.65 ± 0.11	12.1 ± 0.5	78.4 ± 11.8	10.73 ± 0.79	2127 ± 111
RT Aql.....	1996 Jun 3	9.5	0.50 ± 0.12	9.0 ± 0.5	101.7 ± 15.2	7.24 ± 0.51	2763 ± 125
V Cam.....	1996 Oct 9	13.0	0.63 ± 0.10	12.4 ± 0.5	79.1 ± 11.9	8.36 ± 0.52	2414 ± 86
V Cas	1996 Oct 6	10.8	1.88 ± 0.20	8.9 ± 0.6	28.6 ± 4.3	6.30 ± 0.71	2157 ± 146
Y Cas	1996 Oct 7	11.2	0.47 ± 0.20	10.7 ± 0.6	97.4 ± 14.6	7.28 ± 0.66	2727 ± 160
S CrB	1996 Mar 7	10.4	-0.07 ± 0.03	10.5 ± 0.4	160.5 ± 24.1	11.35 ± 0.52	2473 ± 46
R CVn.....	1996 Mar 13	8.5	0.01 ± 0.46	8.5 ± 0.8	134.8 ± 20.2	7.66 ± 0.41	2882 ± 90
	1996 May 29	10.5	0.14 ± 0.05	10.4 ± 0.4	162.9 ± 24.4	6.63 ± 0.64	3248 ± 200
BG Cyg.....	1996 Jun 7	11.5	1.05 ± 0.12	10.5 ± 0.5	57.9 ± 8.7	4.14 ± 0.84	3175 ± 344
DG Cyg	1996 May 29	11.0	1.18 ± 0.20	9.8 ± 0.6	52.6 ± 7.9	5.36 ± 0.69	2723 ± 204
R Dra.....	1997 Jul 5	11.3	0.66 ± 0.14	10.6 ± 0.5	82.6 ± 12.4	12.04 ± 1.44	2034 ± 139
RU Her.....	1996 Jun 2	11.3	0.25 ± 0.12	11.0 ± 0.5	114.7 ± 17.2	8.71 ± 0.52	2596 ± 109
U Her.....	1996 Jun 2	10.3	-0.04 ± 0.13	10.3 ± 0.5	158.9 ± 23.8	11.18 ± 0.75	2486 ± 125
R LMi.....	1996 Mar 7	13.0	-0.16 ± 0.06	13.2 ± 0.4	158.6 ± 23.8	14.40 ± 0.87	2189 ± 87
RT Oph.....	1996 Jun 7	14.0	2.03 ± 0.50	12.0 ± 0.8	22.1 ± 3.3	6.52 ± 0.69	1989 ± 129
UU Peg.....	1996 Jun 3	13.8	0.82 ± 0.15	12.9 ± 0.5	64.9 ± 9.7	9.56 ± 0.68	2149 ± 111
Z Peg.....	1996 Oct 4	9.3	1.24 ± 0.20	8.0 ± 0.6	53.7 ± 8.0	4.50 ± 0.73	2987 ± 267
RR Per.....	1996 Oct 7	13.1	1.50 ± 0.20	11.6 ± 0.6	36.5 ± 5.5	6.83 ± 0.66	2202 ± 135
U Per	1996 Oct 6	9.3	1.05 ± 0.20	8.2 ± 0.6	63.3 ± 9.5	5.41 ± 0.78	2839 ± 230
BG Ser	1996 Jun 4	11.9	0.38 ± 0.19	11.5 ± 0.5	103.1 ± 15.5	6.71 ± 0.83	2879 ± 207
S Ser.....	1996 Mar 11	11.8	2.03 ± 0.26	9.8 ± 0.6	26.9 ± 4.0	5.35 ± 0.84	2305 ± 201
	1996 Jun 8	11.8	2.03 ± 0.45	9.8 ± 0.7	24.1 ± 3.6	5.51 ± 0.48	2209 ± 106
S UMi	1996 Jun 6	10.2	-0.09 ± 0.15	10.3 ± 0.5	166.4 ± 25.0	7.98 ± 0.93	2977 ± 206
RS Vir.....	1996 Jun 10	13.2	1.36 ± 0.20	11.8 ± 0.6	41.2 ± 6.2	7.54 ± 0.74	2160 ± 133
R Cas[a].....	1995 Oct 4	11.1	-1.29 ± 0.13	12.4 ± 0.4	447.4 ± 85.2	$23.03^{+2.13}_{-4.13}$	2239^{+152}_{-236}

[a] R Cas data is reanalysis of visibility data from van Belle et al. 1996.

able as direct indicators of the true photospheric diameters of Mira variables (Willson 1986), although contrasting with the possibility that extended atmospheric constituents might affect the apparent stellar size (Bedding et al. 2001). As we shall see in § 4, this appears to be more than a mere possibility.

In our previous article on Miras observed at IOTA (van Belle et al. 1996), we used a phase-dependent scaling as derived from Scholz & Takeda (1987), ranging from 0.98 at maximum light to 1.11 at minimum light. For this article, we decided to use a constant scaling in order to increase our sensitivity to true size and temperature variations, rather than variations derived from varying scaling factors. Our UD diameters from van Belle et al. (1996) were rescaled using the 1.00 ± 0.04 value above as well.

We also note that some consideration was given to the possibility of departures from spherical symmetry in these variable stars. As has been observed in visible light observations of Mira variables (Karovska et al. 1991; Haniff et al. 1992; Wilson et al. 1992; Weigelt et al. 1996; Tuthill, Haniff, & Baldwin 1999a), these stars can be considerably elongated, possessing up to a 20% difference between semimajor and semiminor axes, although this appears to diminish at 1.0 μm (Hofmann et al. 2000). Similar observations at 2.2 μm have indicated that this elongation is potentially present in the near-IR as well, with asymmetries of up to 25% (Tuthill et al. 2000; Thompson, Creech-Eakman, & Akeson 2002a). Such K-band asymmetries potentially could be explained in terms of high-layer water or other molecular contamination seen to be present in models at certain combinations of parameters and phase cycle (Bedding et al. 2001; Scholz 2001) and are consistent with recent observations of Miras using 0.1 μm bands across the K-band window (Thompson et al. 2002b). The reader should be aware of the potential for this effect to introduce spread in our sample of angular sizes, although it is our expectation that its magnitude will be no greater than the errors in the data set.

3.4. *Effective Temperature*

The stellar effective temperature, $T_{\rm eff}$, is defined in terms of the star's luminosity and radius by $L = 4\pi\sigma R^2 T_{\rm eff}^4$. Rewriting this equation in terms of angular diameter and bolometric flux, a value of $T_{\rm eff}$ was calculated from the flux and Rosseland diameter using

$$T_{\rm eff} = 2341 \left(F_{\rm bol}/\theta_R^2\right)^{1/4} . \quad (2)$$

The units of $F_{\rm bol}$ are 10^{-8} ergs cm^{-2} s^{-1}, and θ_R is in mas. The error in $T_{\rm eff}$ is calculated from the usual propagation of errors applied to equation (2). The measured $T_{\rm eff}$ values are given in column (8) of Table 2 and are found to fall in the range between 2000 and 3250 K.

3.5. *Linear Radius*

In order to establish a linear radius from the angular size data presented herein, a distance estimate to the observed Miras needs to be established. Unfortunately, such an estimate can be rather contentious, particularly with the implications upon pulsation mode as can be seen in Haniff et al. (1995) and van Belle et al. (1996). Herein, we shall consider

the infrared period-luminosity relationship of Feast et al. (1989) as considered by Willson (2000). In this review, the relationship is seen to fall in two roughly linear relationships for short- and long-period Miras, which can be expressed as a function of absolute K magnitude:

$$M_{K=}\begin{cases} -3.66\log P + 1.42\,, & \text{for } P > 400\,, \\ -6.94\log P + 10.0\,, & \text{for } P < 400\,. \end{cases} \quad (3)$$

The above period-luminosity relationship carries the implicit assumption that all Miras are pulsating in the same mode; given the variability of Miras at K and other uncertainties in this relationship, we shall assume that distances derived from it have 25% errors. The results that will be established in § 4 were also considered in light of the K-band period-luminosity relationship given in Whitelock & Feast (2000; $M_K = -3.47 \log P + 0.84$ for all periods), which favored an overtone pulsation mode and resulted in only marginal quantitative (≈4%) and no qualitative differences in § 4. As such, we do not feel that pulsation-mode assumptions that might be inherent in the selected period-luminosity relationship affect our conclusions.

Because of the large standard errors in the *Hipparcos* Mira data set, we will not consider distance metrics derived from the parallaxes for these stars in the otherwise excellent database (e.g., van Leeuwen et al. 1997; Whitelock & Feast 2000). The release of the *Hipparcos* results (Perryman et al. 1997) has provided the community with a wealth of distance data on a variety of stars. For Miras, however, the results were rather unimpressive: the parallaxes showed a great deal of scatter, and the standard errors were large (catalog field H16), on average, 2.2 ± 3.0 mas for the stars presented in this study, which is consistent with the average standard error of 2.6 ± 2.5 mas found for the 172 M type Miras found in Table 1 of Whitelock & Feast (2000).

There are two potential sources for these effect in the *Hipparcos* parallax data: First, a 10 mas object (typical of this study) with an intrinsic size of roughly 350 $R_\odot$ (van Belle et al. 1997) has a parallax of approximately 3 mas: the angular diameter of a Mira variable is about 3 times its parallax, with the standard error on a typical parallax being equal to the measurement itself. Determination of a varying visible light photocenter shift, the bandpass of *Hipparcos* operation, could easily be complicated by this disparity. Second, any spots on the surface of these highly evolved objects could also affect the apparent position of the photocenter (van Leeuwen et al. 1997), although the existence of such spots on Miras has not yet been established empirically. We do not expect this effect to be a function of the typically large distances to the Miras, relative to the majority of stars in the *Hipparcos* data set. A similar examination of the similarly distant 322 northern hemisphere single (multiplicity field H59 and spectral type both indicating no companions) supergiants found in the *Hipparcos* data set indicates a contrasting average standard error of 0.90 ± 0.30 mas; this average standard error appears to be independent of object parallax. Furthermore, the possibility of Lutz-Kelker bias within any given *Hipparcos* sample of stars has been empirically established (Oudmaijer, Groenewegen, & Schrijver 1998) and should be carefully considered.

We have detailed our evaluation of the *Hipparcos* data set at length in this section, given our otherwise positive experience with the catalog's far-reaching utility. As such, we did not wish to dismiss the *Hipparcos* Mira data lightly, but did so only after careful consideration of the data.

3.6. *Reanalysis of R Cas*

One star from van Belle et al. (1996) that bears reexamining is R Cas. In our previous manuscript, a value of $\theta = 13.55 \pm 0.95$ mas was derived from the measured visibility $V = 0.1259 \pm 0.0360$ from 1995 October 4/5. However, for visibilities below $V = 0.132$, the visibility function becomes nonmonotonic and has multiple solutions. Neglected in van Belle et al. (1996) were the other angular sizes possible with this visibility: 19.53 and 22.03 mas. The error envelope about the measured visibility encloses the peak of the entire first outlying lobe; hence, the error envelope for these angular sizes ranges from 17.90 to 24.16 mas.

Based upon visible light angular size measurements of this object (Haniff et al. 1995; Hofmann et al. 2000) that are in the 18 to 36 mas range, the angular size solution most consistent with our previous V measurement is 22.03 mas. We note, though, that for the visibility measurements outside of the central lobe of the visibility function, the influence of limb darkening and spotting becomes greater and reduces the effectiveness of using single-visibility measurements to establish stellar angular sizes, as well illustrated in HSW98.

4. DISCUSSION: SIZE AND PULSATION MODE

Theoretical models for many Mira variables predict their effective temperatures will lie at approximately 3000–3100 K, which is somewhat higher than the values seen in Table 2 (cf. Hoffman et al. 1998; Willson 2000). One possible explanation for this discrepancy is a systematic overestimation of the apparent sizes of the variable stars by the interferometer. Absorption of the central star's flux by molecules will have the effect of contaminating the observed angular sizes and will lead to a 2.2 μm uniform disk size that is markedly larger than the Rosseland mean diameter. A few of the models found in HSW98 show "wings" in the center-to-limb brightness profiles, mainly caused by water molecules (Bedding et al. 2001; Jacob & Scholz 2002), which are consistent with this hypothesis, as are all of the dusty Mira models in Bedding et al. (2001). As discussed in § 3.3, conversion of the observed interferometric visibility to the desired Rosseland $\tau = 1$ radius can run afoul of these wings, causing the inferred size to be dramatically underestimated, as seen in Bedding et al. (2001) and Scholz (2001).

To test this hypothesis, we can examine K–[12] colors for the Miras observed at IOTA. Twelve micron magnitudes are readily available for these stars, as defined in Hickman, Sloan, & Canterna (1995), using flux values for the observed Miras found in the *IRAS* Point Source Catalog (1987). K–[12] is expected to be a reasonable indicator of recent dusty mass loss (Le Sidaner & Le Bertre 1996; Beichman et al. 1990). Given our interest in establishing gross trends in a relative sense between stars of differing K–[12] values, we did not apply point-source corrections to the *IRAS* 12 μm data (Beichman et al. 1988), nor did we attempt to quantify 12 μm variability for these sources, which is potentially present in any Mira variable data set (Little-Marenin, Stencel, & Staley 1996; Creech-Eakman 1997) but should in this context only add scatter to the 12 μm values.

K-band interferometric observations are relatively insensitive to dusty mass loss (although not completely so, as evidenced with VY CMa in Monnier et al. 1999); however, it is entirely plausible that dusty mass loss will be accompanied by a significant increase in the molecular component of circumstellar material. Significant amounts of absorption by molecules in a circumstellar shell above the Rosseland mean radiating surface will have the effect of increasing the derived size of a interferometrically observed Mira variable. Taking a blackbody at the expected temperature of 3000 K, the predicted $K-[12]$ color will be 0.92. By comparison to the observed colors for the individual Miras, we may calculate a $K-[12]$ excess that will be indicative of stellar mass loss. Given the *K*-band variability of these objects, we assigned an average error of ± 0.33 to our derived $K-[12]$ excess values, which is consistent with the observed *K*-band variability of these objects (Whitelock et al. 2000). These data are listed for all the Miras considered in this analysis in Table 3. Examination of our $K-[12]$ data for R Dra indicates a spurious value, the source of which was unclear. This star was dropped from later consideration in the analysis.

TABLE 3

Mira Variable Absolute *K* Magnitudes, Distances, Radii, *IRAS* 12 μm Magnitudes, $K-[12]$ Colors, and Estimated $K-[12]$ Color Excesses

Star	Date	M_K (mag)	Dist. (pc)	Radius ($R_\odot$)	[12] (mag)	$K-[12]$ (mag)	$K-[12]$ Excess (mag)	Ref.
R Aql	1995 Jun 10	−7.55	224	259 ± 67	−2.88	2.04	1.13	1
	1995 Oct 6	−7.55	224	328 ± 85	−2.88	2.11	1.20	1
RR Aql	1996 Jun 4	−8.09	561	648 ± 169	−2.67	3.32	2.41	2
RT Aql	1996 Jun 5	−7.46	392	305 ± 79	−1.05	1.55	0.64	2
R Aqr	1995 Jul 11	−8.05	272	438 ± 114	−4.37	3.36	2.45	1
	1995 Oct 7	−8.05	272	412 ± 106	−4.37	3.63	2.72	1
U Ari	1977 Sep 3	−7.98	779	801 ± 205	−0.99	2.47	1.56	3
R Aur	1995 Oct 3	−8.46	342	407 ± 105	−3.03	2.24	1.33	1
V Cam	1996 Oct 9	−8.87	796	716 ± 185	−2.14	2.77	1.86	2
R Cas	1995 Oct 4	−8.28	250	593 ± 181	−4.19	2.90	1.99	2
T Cas	1995 Oct 4	−8.38	302	416 ± 108	−2.95	1.97	1.06	1
V Cas	1996 Oct 6	−7.33	696	472 ± 129	−0.94	2.82	1.91	2
Y Cas	1996 Oct 7	−8.14	527	413 ± 110	−1.34	1.82	0.91	2
o Cet	1990 Aug 21	−7.80	121	482 ± 124	−5.59	3.39	2.48	4
	1990 Sep 19	−7.80	121	468 ± 120	−5.59	2.99	2.08	4
S CrB	1996 Mar 8	−7.93	375	457 ± 116	−2.13	2.07	1.16	2
R CVn	1996 Mar 13	−7.79	391	279 ± 75	−1.40	1.41	0.50	2
	1996 May 31	−7.79	391	322 ± 82	−1.40	1.74	0.83	2
BG Cyg	1996 Jun 7	−7.57	530	236 ± 76	−0.74	1.79	0.88	2
DG Cyg	1996 May 29	−8.50	865	499 ± 140	...	...	...	2
R Dra	1997 Jul 5	−7.32	395	511 ± 142	0.42	0.24	−0.67	2
RU Her	1996 Jun 2	−8.64	610	572 ± 147	−1.97	2.25	1.34	2
S Her	1995 Jul 7	−7.68	677	354 ± 124	−0.21	1.68	0.77	1
U Her	1995 Jun 10	−8.11	377	431 ± 114	−3.12	2.69	1.78	1
	1996 Jun 2	−8.11	377	453 ± 117	−3.12	3.08	2.17	2
R Leo	1990 May 2	−7.81	115	409 ± 105	−4.71	2.21	1.30	5
R LMi	1996 Mar 7	−7.98	367	569 ± 146	−2.94	2.78	1.87	2
RT Oph	1996 Jun 7	−8.26	1142	801 ± 217	−0.80	2.83	1.92	2
X Oph	1995 Jul 7	−7.80	225	314 ± 81	−2.90	1.87	0.96	1
	1995 Oct 7	−7.80	225	298 ± 78	−2.90	1.85	0.94	1
S Ori	1995 Jul 7	−8.30	481	545 ± 142	−1.82	1.93	1.02	1
U Ori	1995 Oct 8	−7.98	310	370 ± 96	−3.45	2.93	2.02	1
R Peg	1995 Jul 7	−8.00	435	476 ± 122	−2.03	2.53	1.62	1
	1995 Oct 6	−8.00	435	455 ± 119	−2.03	1.85	0.94	1
S Peg	1995 Oct 6	−7.74	675	459 ± 135	−0.37	1.82	0.91	1
	1995 Jul 8	−7.74	675	574 ± 154	−0.37	1.73	0.82	1
UU Peg	1996 Jun 3	−8.47	721	742 ± 193	−1.89	2.71	1.80	2
Z Peg	1996 Oct 4	−7.80	640	310 ± 92	−0.70	1.93	1.02	2
RR Per	1996 Oct 7	−8.06	816	599 ± 161	−0.76	2.26	1.35	2
U Per	1995 Oct 4	−7.73	559	352 ± 101	−0.66	1.63	0.72	1
	1996 Oct 6	−7.73	559	325 ± 94	−0.66	1.71	0.80	2
BG Ser	1996 Jun 4	−8.07	491	354 ± 99	−1.56	1.94	1.03	2
R Ser	1995 Jul 7	−7.91	356	328 ± 86	−2.07	1.92	1.01	1
S Ser	1996 Mar 11	−8.00	1012	601 ± 159	−0.45	2.48	1.57	2
	1996 Jun 8	−8.00	1012	583 ± 172	−0.45	2.48	1.57	2
S UMi	1996 Jun 6	−7.78	345	296 ± 82	−1.78	1.69	0.78	2
RS Vir	1996 Jun 10	−7.90	712	577 ± 155	−1.46	2.82	1.91	2

References.—(1) van Belle et al. 1996; (2) this work; (3) Ridgway et al. 1979; (4) Ridgway et al. 1992; (5) di Giacomo et al. 1991.

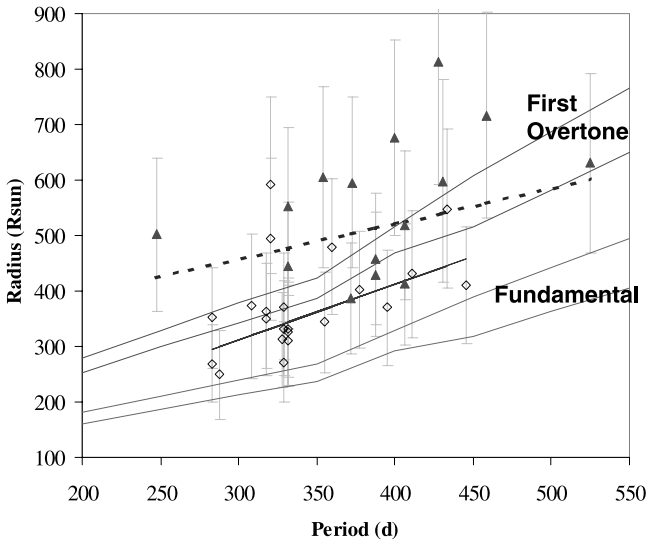

FIG. 1.—Radius vs. period for the Miras observed. Open diamonds are for Miras with $K-[12]$ excess between +0.0 and +1.25, indicating less dusty mass loss, and filled triangles are for Miras with $K-[12]$ excess greater than +1.75, indicating more lass loss. Comparing fit lines for the lower and higher mass loss Miras (*solid and dotted lines*, respectively), the Miras with greater dusty mass loss appear on average 120 $R_\odot$ larger. The fundamental and first-overtone regions are derived from the radius-period relationships found in Ostlie & Cox (1986). See § 4 for details of the line fits. [*See the electronic edition of the Journal for a color version of this figure.*]

The observed Miras were separated into two sets: those with small values of $K-[12]$ excess, between 0 and 1.25, which will be indicative of Miras with lower mass loss rates, and those with $K-[12]$ excess greater than 1.75, indicative of the higher mass loss rate Miras; stars in the intermediate $K-[12]$ range were not considered for this specific analysis (although they were a part of the analysis associated with Fig. 2, as shown later in this section). A plot of this is seen in Figure 1, where the stars with low mass loss show systematically smaller sizes than those with the more substantial mass loss; stars with multiple entries in Table 3 are represented by a corresponding number of data points in Figure 1. Fitting a line to each of the two data sets, we find that $R = (1.01 \pm 0.50)P + (10 \pm 170)\ R_\odot$ for those Miras with little $K-[12]$ excess (line fit $\chi^2_\nu = 0.41$) and $R = (0.63 \pm 0.64)P + (270 \pm 245)\ R_\odot$ for the Miras with $K-[12]$ excess greater than 1.75 ($\chi^2_\nu = 0.61$). Averaging over periods of 300–450 days, we find that the higher mass loss Miras appear, on average, 120 $R_\odot$ (roughly 30%) larger than their lower mass loss counterparts across all periods, with this difference ranging from 145 to 90 $R_\odot$ as the period increases from $P = 275$ to 450 days. This correlation of increased radius with $K-[12]$ excess is a clear indication that the sizes we derive from our interferometric observations progressively overestimate the Rosseland mean diameters for these objects as mass loss increases. Noting the discussion in § 3.5, this result is independent of pulsation-mode assumptions.

Futhermore, the direction of that progression appears to indicate that our diameters are systematically biased toward larger sizes, which is consistent with the effects of a circumstellar shell upon the interferometric observables. The presence of circumstellar structures substantial enough to be seen in our interferometric data will grossly invalidate our assumptions regarding interpretation of the visibility data in terms of a scaled uniform disk size and tend to systematically increase the derived stellar disk size at all spatial frequencies (Bedding et al. 2001; Scholz 2001).

Once we have established $K-[12]$ color excess dependency for the Mira radii in our sample, we may inspect it to see if there is a correlation between $K-[12]$ excess and inferred radius, using the inferred radius as a function of period to then inspect the indicated pulsation mode. As discussed in § 3.5, the selected period-luminosity relationship has little bearing upon the resultant sizes, and, as such, any assumption of pulsation mode inherent in the referenced period-luminosity relationships does not appear to alter our results. For this purpose, we used the pulsation-mode–dependent radius-period relationships as found in Ostlie & Cox (1986):

$$1.86 \log R = 0.73 \log M + 1.92 + \log P \quad \text{(for fundamental)}, \tag{4}$$

$$1.59 \log R = 0.51 \log M + 1.60 + \log P \quad \text{(for first overtone)}. \tag{5}$$

Additionally, for the purposes of using this relationship, we shall adopt period-dependent masses, as illustrated in Figure 5 of Willson (2000), with a range of 15% in mass versus period for $P \leq 400$ days (increasing from 0.7 to 1 $M_\odot$ with period) and a range of 25% in mass versus period for $P > 400$ days (1–4 $M_\odot$). Although this use of a relationship derived from linear rather than nonlinear modeling might be questionable (Barthes 1998; Ya'ari & Tuchman 1999), it shall be sufficient to establish the dependence of the measured radii upon mass-loss rates. Having established these theoretical mode-dependent regions, we may inspect our data in reference to the fundamental and first-overtone regions, also seen in Figure 1. There are two striking characteristics to this aspect of the figure; first, the tendency for the Miras with large $K-[12]$ color excesses to lie in the first-overtone region; and second, all of the stars lie above the region defined by the fundamental-overtone lines. Both of these aspects are consistent with apparent size overestimation due to circumstellar shell contamination of the visibility data.

Taking the sizes from the Ostlie & Cox (1986) fundamental-mode relationship and establishing predicted sizes for all of the stars in our data set, we may plot the observed-to-predicted size ratio versus the $K-[12]$ excess numbers for all of the Miras in our data set, as seen in Figure 2. There is a clear progression from smaller to larger positive residuals as the excess increases, with predicted scaling being in excess of 1.0 for all observed stars (excepting R Dra, as noted above). A similar exercise may be carried out in light of the first-overtone predictions, but this results in a scaling factor of less than 1.0 for stars with $K-[12]$ excess less than 1.50, which is more than half of our data set. Scalings less than unity are inconsistent with size enhancement due to circumstellar absorption. It is possible other physical phenomena could appear to decrease the size of the stars when viewed by the interferometer, e.g., bright spots, but this explanation is unlikely for two reasons. First, structures at spatial scales smaller than the gross size of the star will need to satisfy a fortuitous geometry to properly affect our visibility data. While this is possible for specific examples in our data set, it seems doubtful that this would present itself as a general effect across our entire ensemble of data. Second, it is

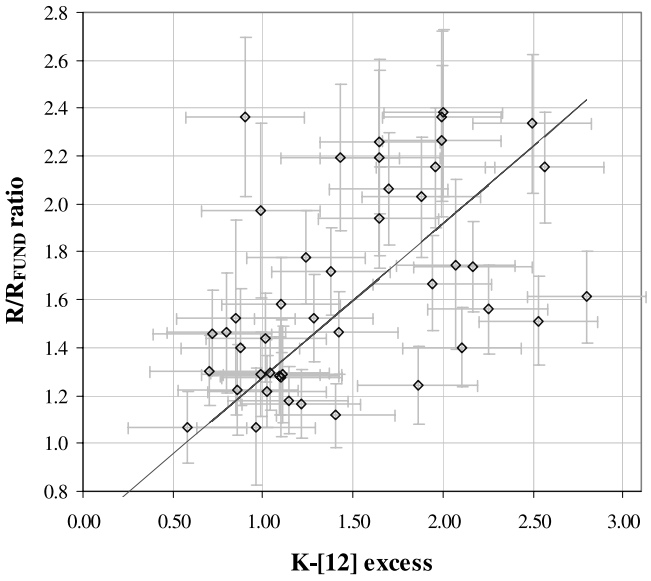

FIG. 2.—Ratio of observed radius to predicted fundamental-mode radius vs. $K-[12]$ excess. [*See the electronic edition of the Journal for a color version of this figure.*]

unlikely that such structures will have sufficient contrast at 2.2 μm to significantly affect the interferometric observables—for a 10% increase in size, a spot would have to be 33% the diameter of the star, properly aligned, and 1000 K hotter than the surrounding photosphere. Both the size and temperature differential of such a spot do not seem credible.

Adjusting the angular diameters by this $K-[12]$ excess-dependent scaling factor results in the average inferred effective temperature rising from 2500 to 3200 K, which is more consistent with the expected effective temperature value for these stars at the Rosseland mean radiating surface when they are pulsating in the fundamental mode (HSW98; Willson 2000).

Measurements of the angular size of Mira at a variety of wavelengths by other groups appears to support this hypothesis. At 2.2 μm, the 36.1 ± 1.4 mas size measured by Ridgway et al. (1992) is in agreement with a similar recent measurement of 31.6 mas at 2.26 μm by Tuthill, Monnier, & Danchi (1999b; no error or phase was given in this promising but preliminary result). However, at 11.15 μm, Weiner et al. (2000) find an angular size of 47.8 ± 0.5 mas. This larger size is consistent with the presence of a circumstellar dust shell, which is, in turn, consistent with the $K-[12]$ excess value that we compute to be in excess of 2 mag (see Table 3). Furthermore, Tuthill et al. (1999b) also measured the angular size of Mira at a variety of other wavelengths: $\theta(1.24\ \mu\text{m}) = 23.3$ mas, $\theta(1.65\ \mu\text{m}) = 28.3$ mas, and $\theta(3.08\ \mu\text{m}) = 59.9$ mas. The increased K-band size relative to the J-band size appears to be consistent with our expectation that the K-band sizes are being enhanced by the presence of circumstellar material.

5. CONCLUSIONS

The IOTA program of observing Mira variable stars has resulted in a substantial increase in the number of near-infrared angular size measurements for Miras; previous results were available for ≈25 of these stars. Determinations of $T_{\rm eff}$ and R are possible, with the caveat that the derived Rosseland mean radius values are potentially overestimated because of circumstellar shells. The atmospheric models that are used in reducing the visibility data clearly play a significant role in the results obtained. Our data are consistent with at least some of the observed Mira variables pulsating in the fundamental mode. For those Miras that appear to be too large to be pulsating in the fundamental mode, there appears to be a correlation between $K-[12]$ color excess and size, reflective of mass loss enhancing the apparent size. If our inference that molecular absorption about the Miras is responsible for an increased apparent K-band size of these objects, a number of effects should be observable, the most noticeable of which will be the size of the Miras, which will appear to be smaller in the J and H bands than in the K band, where such absorption is less. The preliminary results of Tuthill et al. (1999b) appear to support this conclusion. We predict that an angular size pulsation-mode study of these objects carried out at 1.6 μm or particularly 1.2 μm will result in unequivocal evidence for fundamental-mode pulsation for most, if not all, Miras.

We would like to thank the staff at the Center for Astrophysics for a generous allotment of telescope time so that this project could be carried out, and Ron Canterna for liberal use of computer resources for data reduction. We acknowledge particularly fruitful discussions with Michael Scholz and Lee Anne Willson. This research has been partially supported by NSF grant AST 90-21181 to the University of Wyoming, the Wyoming Space Grant Consortium, and NASA grant NGT-40050. This research has made use of the SIMBAD database and the AFOEV database, both operated by the CDS, Strasbourg, France. In this research, we have used, and acknowledge with thanks, data from the AAVSO International Database, based on observations submitted to the AAVSO by variable star observers worldwide. Portions of this work were performed at the Jet Propulsion Laboratory, California Institute of Technology, under contract with the National Aeronautics and Space Administration.

REFERENCES

Alvarez, R., & Mennessier, M.-O. 1997, A&A, 317, 761
Barthes, D. 1998, A&A, 333, 647
Bedding, T. R., Jacob, A. P., Scholz, M., & Wood, P. R. 2001, MNRAS, 325, 1487
Beichman, C. A., Chester, T., Gillett, F. C., Low, F. J., Matthews, K., & Neugebauer, G. 1990, AJ, 99, 1569
Beichman, C. A., Neugebauer, G., Habing, H. J., Clegg, P. E., & Chester, T. J. 1988, IRAS Catalogs and Atlases, Version 2, Explanatory Supplement (NASA RP-1190) (Washington: GPO)
Bessell, M. S., Scholz, M., & Wood, P. R. 1996, A&A, 307, 481
Blackwell, D. E., & Lynas-Gray, A. E. 1994, A&A, 282, 899
Bowen, G. H. 1988, ApJ, 329, 299
Bowen, G. H., & Willson, L. A. 1991, ApJ, 375, L53
Burns, D., et al. 1998, MNRAS, 297, 462
Carleton, N. P., et al. 1994, Proc. SPIE, 2200, 152
Colavita, M. M., et al. 1999, ApJ, 510, 505
Creech-Eakman, M. J. 1997, Ph.D. thesis, Univ. Denver
di Giacomo, A., Lisi, F., Calamai, G., & Richichi, A. 1991, A&A, 249, 397
Dyck, H. M., et al. 1995, AJ, 109, 378
Dyck, H. M., Benson, J. A., van Belle, G. T., & Ridgway, S. T. 1996, AJ, 111, 1705
Dyck, H. M., Lockwood, G. W., & Capps, R. W. 1974, ApJ, 189, 89
Feast, M. W., Glass, I. S., Whitelock, P. A., & Catchpole, R. M. 1989, MNRAS, 241, 375
Gezari, D. Y., Schmitz, M., Pitts, P. S., & Mead, J. M. 1993, Catalog of Infrared Observations (NASA RP-1294) (3d ed.; Washington: NASA)

Groenewegen, M. A. T. 2000, A&A, 363, 901
Groenewegen, M. A. T., & Salaris, M. 2001, A&A, 366, 752
Haniff, C. A., Ghez, A. M., Gorham, P. W., Kulkarni, S. R., Matthews, K., & Neugebauer, G. 1992, AJ, 103, 1662
Haniff, C. A., Scholz, M., & Tuthill, P. G. 1995, MNRAS, 276, 640
Hickman, M. A., Sloan, G. C., & Canterna, R. 1995, AJ, 110, 2910
Hill, S. J., & Willson, L. A. 1979, ApJ, 229, 1029
Hoffleit, D., & Jaschek, C. 1982, The Bright Star Catalog (4th ed.; New Haven: Yale Univ. Press)
Hofmann, K.-H., Balega, Y., Scholz, M., & Weigelt, G. 2000, A&A, 353, 1016
Hofmann, K.-H., et al. 2002, NewA, 7, 9
Hofmann, K.-H., Scholz, M., & Wood, P. R. 1998, A&A, 339, 846
Horne, J. H., & Baliunas, S. L. 1986, ApJ, 302, 757
IRAS Catalog of Point Sources, Version 2.0. 1987, Joint *IRAS* Science Working Group (Washington: GPO)
Jacob, A. P., & Scholz, M. 2002, in preparation
Karovska, M., Nisenson, P., Papaliolios, C., & Boyle, R. P. 1991, ApJ, 374, L51
Kholopov, P. N., et al. 1985, General Catalog of Variable Stars (4th ed.; Moscow: Nauka)
Lattanzi, M. G., Munari, U., Whitelock, P. A., & Feast, M. W. 1997, ApJ, 485, 328
Le Sidaner, P., & Le Berte, P. 1996, A&A, 314, 896
Little-Marenin, I. R., Stencel, R. E., & Staley, S. B. 1996, ApJ, 467, 806
Lockwood, G. W. 1972, ApJS, 24, 375
Lockwood, G. W., & Wing, R. F. 1971, ApJ, 169, 63
Mathis, J. S. 1990, ARA&A, 28, 37
Monnier, J. D., Tuthill, P. G., Lopez, B., Cruzalebes, P., Danchi, W. C., & Haniff, C. A. 1999, ApJ, 512, 351
Nelson, C. A., Cook, K. H., Popowski, P., & Alves, D. R. 2000, AJ, 119, 1205
Neugebauer, G., & Leighton, R. B. 1969, Two-Micron Sky Survey (NASA SP-3047) (Washington: NASA)
Ostlie, D. A., & Cox, A. N. 1986, ApJ, 311, 864
Oudmaijer, R., Groenewegen, M. A. T., & Schrijver, H. 1998, MNRAS, 294, L41
Perl, M., & Tuchman, Y. 1990, ApJ, 360, 554
Perrin, G., Coudé du Foresto, V., Ridgway, S. T., Mennesson, B., Ruilier, C., Mariotti, J.-M., Traub, W. A., & Lacasse, M. G. 1999, A&A, 345, 221
Perryman, M. A. C., et al. 1997, The Hipparcos and Tycho Catalogs (ESA SP-1200) (Noordwijk: ESA)
Ribas, I., et al. 2000, ApJ, 528, 692
Ridgway, S. T., Benson, J. A., Dyck, H. M., Townsley, L. K., & Hermann, R. A. 1992, AJ, 104, 2224
Ridgway, S. T., Wells, D. C., Joyce, R. R., & Allen, R. G. 1979, AJ, 84, 247
Rowan-Robinson, M., & Harris, S. 1983, MNRAS, 202, 767
Scargle, J. D. 1982, ApJ, 263, 835
Scholz, M. 2001, MNRAS, 321, 347
Scholz, M., & Takeda, Y. 1987, A&A, 186, 200
Thompson, R. R., Creech-Eakman, M. J., & Akeson, R. L. 2002, ApJ, 570, 373
Thompson, R. R., Creech-Eakman, M. J., & van Belle, G. T. 2002, ApJ, in press
Tuchman, Y., Sack, N., & Barkat, Z. 1979, ApJ, 234, 217
Tuthill, P. G., Danchi, W. C., Hale, D. S., Monnier, J. D., & Townes, C. H. 2000, ApJ, 534, 907
Tuthill, P. G., Haniff, C. A., & Baldwin, J. E. 1999a, MNRAS, 306, 353
Tuthill, P. G., Monnier, J. D., & Danchi, W. C. 1999b, in ASP Conf. Ser. 194, Working on the Fringe: Optical and IR Interferometry from Ground and Space, ed. Stephen Unwin & Robert Stachnik (San Francisco: ASP), 188
van Belle, G. T., Dyck, H. M., Benson, J. A., & Lacasse, M. G. 1996, AJ, 112, 2147
van Belle, G. T., Dyck, H. M., Thompson, R. R., Benson, J. A., & Kannappan, S. J. 1997, AJ, 114, 2150
van Leeuwen, F., Feast, M. W., Whitelock, P. A., & Yudin, B. 1997, MNRAS, 287, 955
Weigelt, G., Balega, Y., Hofmann, K.-H., & Scholz, M. 1996, A&A, 316, L21
Weiner, J., Danchi, W. C., Hale, D. D. S., McMahon, J., Townes, C. H., Monnier, J. D., & Tuthill, P. G. 2000, ApJ, 544, 1097
Whitelock, P. A., & Feast, M. W. 2000, MNRAS, 319, 759
Whitelock, P. A., Marang, F., & Feast, M. W. 2000, MNRAS, 319, 728
Willson, L. A. 1986, in Late Stages of Stellar Evolution, ed. S. Kwok & S. R. Pottasch (Dordrecht: Reidel), 253
———. 2000, ARA&A, 38, 573
Willson, L. A., & Hill, S. J. 1979, ApJ, 228, 854
Wilson, R. W., Baldwin, J. E., Buscher, D. F., & Warner P. J. 1992, MNRAS, 257, 369
Wood, P. R. 1974, ApJ, 190, 609
———. 1990, in From Miras to Planetary Nebulae: Which Path for Stellar Evolution?, ed. M. O. Mennessier & A. Omont (Gif-sur-Yvette: Ed. Frontières), 67
Wood, P. R. 2000, Publ. Astron. Soc. Australia, 17, 18
Wood, P. R., et al. 1999, in IAU Symp. 191, Asymptotic Giant Branch Stars, ed. T. Le Berte, A. Lebre, & C. Waelkens (San Francisco: ASP), 151
Ya'ari, A., & Tuchman, Y. 1999, ApJ, 514, L35
Young, J. S., et al. 2000, MNRAS, 318, 381